Small-Angle X-ray Contrast-Variation Study of Micelles Formed by Poly(styrene)−Poly(ethylene oxide) Block Copolymers in Aqueous Solution

P. Hickl and M. Ballauff*

Polymer-Institut, Universität Karlsruhe, Kaiserstrasse 12, 76128 Karlsruhe, Germany

A. Jada

Ecole Nationale Supérieure de Chimie, 3 rue Werner, 68093 Mulhouse Cedex, France

Received October 2, 1995[⊗]

ABSTRACT: A small-angle X-ray scattering (SAXS) study of micelles formed by a symmetric block copolymer consisting of poly(styrene) and poly(ethylene oxide) (molecular weight of each block: 1000 g/mol; concentration up to 15.4 wt %) is given. The contrast of the micelles toward water was changed by adding glycerol to the solution. The analysis of the SAXS data shows that the addition of glycerol does not change the structure of the micelles. With the aid of contrast variation, SAXS allows determination of the following integral parameters: (i) the mean electron density of the particle $\bar{\rho}$ together with the particle volume V_p, (ii) the radius of gyration at infinite contrast $R_{g,\infty}$ together with the inhomogeneity parameter α, and (ii) the volume V_c related to the shape of the particles as well as parameters characterizing the internal density fluctuation of the particles. Furthermore the correlation length l_c has been determined as a function of concentration and contrast. A comparison of these parameters and of the scattering intensities at various contrast with concentric models of the radial electron density shows the following: The micelles have an overall spherical shape and a narrow size distribution (weight-average aggregation number = 400; standard deviation of the size distribution 10.9%). The unpolar component poly(styrene) together with a fraction of the polar poly(ethylene) blocks is located in the core.

Introduction

Block copolymers consisting of two polymers widely differing in polarity may form micelles in suitable solvents.[1] These systems present interesting examples of self-organization studied extensively during the recent decades.[1,2] Since the pioneering work of Plestil and Baldrian[3] small-angle X-ray scattering (SAXS) as well as small-angle neutron scattering (SANS) has been applied frequently for the study of the internal structure and the interaction of such micelles. A survey of these investigations may be found in the recent reviews by Chu[4] and by Almgren et al.[5] The main goal of most of these studies is the determination of the shape of the micelles as well as of their internal architecture for comparison with theoretical models.[6] In a polar solvent the hydrophobic part of the block copolymer will form the core of such micelles, whereas the hydrophilic block is expected to extend into the polar phase. The outer shell thus may be described in first approximation as chains anchored onto a convex spherical surface[7] and may be compared[8] to the structure of star polymers.[9]

Very often the data provided by the small-angle scattering experiment only suffice to model the internal structure in terms of a concentric core−shell model (see, e.g., the discussion of this point in the review by Chu[4]). On the other hand, a SAXS or SANS study is in principle suited to give more detailed information on the internal structure provided that the polydispersity is not too high.[10] In particular, it should be possible to distinguish between the contributions to the scattering intensity due to the shape of the micelles and those due to their internal structure.

In this paper we present the results of a SAXS-study on symmetric block copolymers consisting of poly(styrene) and poly(ethylene oxide) dissolved in water. The choice of this material derives from the fact that its micellization has been studied recently by Xu et al.[11] in great detail. These investigations have demonstrated that this system forms micelles suited for a detailed structural investigation. As demonstrated by a previous study on a related system[12] the electron density of micellar structures composed of styrene and ethylene oxide units can be easily matched by adding glycerol to the solution. Therefore it should be possible to conduct a study employing the technique of contrast variation.[13,14] The dependence of integral parameters[15,16] on contrast allows one to check whether the form and the internal structure of the micelles is changed by the glycerol. SAXS in conjunction with contrast variation has recently been applied successfully to a number of colloidal systems[10,12,17,18] and should in principle allow a determination of both the shape and the internal structure of micellar systems.

Following the prescription of Feigin and co-workes[13,19] the analysis of the micellar structure presented herein takes into account the finite resolution of the SAXS data. Thus, the SAXS intensities have been treated by assuming a continuous shape function.[19] As shown recently[20] this analysis is necessary to account for the presence of morphological details such as the polymer chains in the corona of the micelles.

In addition to this, the dependence of the scattering intensity in the region of lowest angles on concentration will yield the structure factor of the system, which may be evaluated in terms of hard-sphere interactions of the micelles.[21]

Experimental Section

Materials. Glycerol (DAB 7) was used without further purification. For measurements of the partial specific volume of poly(ethylene oxide), three samples of this polymer (M =

* To whom all correspondence should be addressed.

[⊗] Abstract published in *Advance ACS Abstracts,* May 1, 1996.

S0024-9297(95)01480-X CCC: $12.00

1.000, 4.000, and 20.000) were purchased from Aldrich and used without further purification. The poly(styrene)−poly(ethylene oxide) block copolymer SE10 was supplied by Goldschmidt AG and was used as received. A 20 wt % stock solution of the block copolymer was prepared as described by Xu et al.[11] by dissolving a known amount of material in water at 60 °C. After stirring for 1 h at this temperature, the solution is cooled down to room temperature. The clear stock solution was diluted with distilled water or glycerol/water mixtures to obtain concentrations between 0.6 vol % and 15.4 vol %.

Partial Specific Volume. The densities of the block copolymer solutions were determined by a Paar DMA-60 apparatus. Plots of the density vs weight fraction turned out to be strictly linear up to 17 wt %. The resulting partial specific volume is 0.888 cm^3/g.

The partial volume of poly(ethylene oxide) in water at 25 °C measured in the same way is 0.842 cm^3/g (literature:[22] 0.834 cm^3/g). By measuring different molecular weights, it was ensured that the partial specific volume is independent of chains length.

Small-Angle X-ray Scattering. The SAXS intensities were measured by a Kratky-Kompakt-Kamera equipped with a position-sensitive counter. The samples are confined in a capillary mounted on a sample holder within the camera (supplied by the Paar KG, Graz, Austria). The details of the measurements and desmearing of the data have been described elsewhere.[17,23] All intensities reported herein are normalized to the scattering intensity of a single electron. In all cases absolute intensities have been obtained by using the moving-slit method of Stabinger and Kratky.[24] Every sample was measured at least 2 times to lower the statistical errors and to check possible fluctuations of the primary beam intensity.

Figure 1 shows typical examples of smeared scattering intensities as function of the magnitude of the scattering vector q ($q = (4\pi/\lambda)\sin(\theta/2)$; θ, scattering angle) taken from the micellar solution (upper curves) and the respective blank sample without the block copolymer. Here Figure 1a refers to the best possible contrast using water as solvent, whereas Figure 1b displays the respective scattering intensities near the match point (33.9 wt % glycerol). The side maxima of the scattering curves are clearly discernible, even near the match point where the scattering intensity of the micelles is rather low. The solid lines in Figure 1 are spline fits of the measured data, which were used for further evaluations.

The scattering contribution due to the solvent and the sample holder is subtracted according to (cf. ref 23)

$$I(q) = I_m(q) - (1 - \phi)I_{bg}(q) - \phi I_{cap}(q) \qquad (1)$$

where $I_m(q)$ denotes the measured scattering intensity of the sample at a given volume fraction ϕ, $I_{bg}(q)$ is the scattering intensity of the capillary filled with the dispersion medium (water or mixtures of water and glycerol), and $I_{cap}(q)$ is the scattering contribution of the empty capillary. Before subtraction the scattering contributions were corrected to the same center of gravity of the primary beam. Since the background caused by the solvent is the main contribution to the scattering intensity at high scattering angles, its careful removal is of utmost importance for the subsequent discussion.

The background due to density fluctuations has been determined by the empirical fit procedure of the smeared data as proposed by Ruland[25]

$$I(q) = A \exp(Bq^2) \qquad (2)$$

The alternative procedure using Porod's law[15] is not admissible since the scattering curves are structured up to high q-values. At ever higher scattering angles a fit assuming a background independent of q is not possible. This is directly obvious from Figure 2 which shows an example of the fit of eq 2 to experimental data.

It is obvious that in the q-range used for fitting the parameters A and B of eq 2 ($3 < q < 5$ nm^{-1}) the scattering intensity is fully determined by the density fluctuations, which depend on q. Up to $q = 1$ nm^{-1}, however, this contribution is nearly negligible. Errors inferred from the subtraction of the background will only disturb quantities deriving from integrals over the entire range of q, i.e., the determination of the invariant Q (see below).

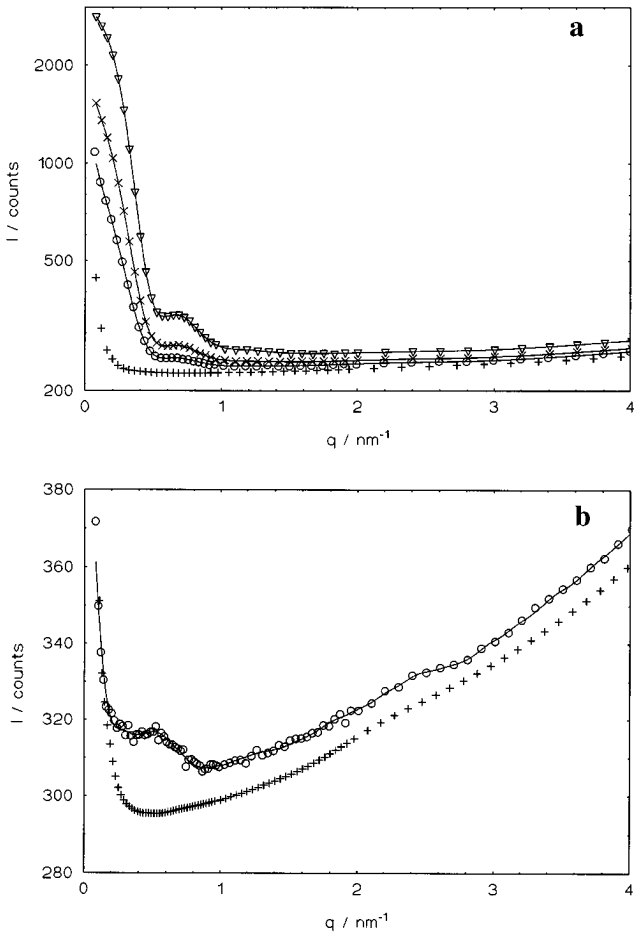

Figure 1. Comparison of the raw data of samples and background. (a) Smeared scattering data of the block copolymers in water measured at different volume fractions ϕ. ○, 0.009; ×, 0.017, ▽, 0.042; +, background of the water-filled capillary. For the sake of clarity only every fourth point is plotted. (b) smeared scattering data measured at 33% glycerol, i.e., near the matchpoint. +: background of the water-filled capillary. For the sake of clarity only every second point is plotted.

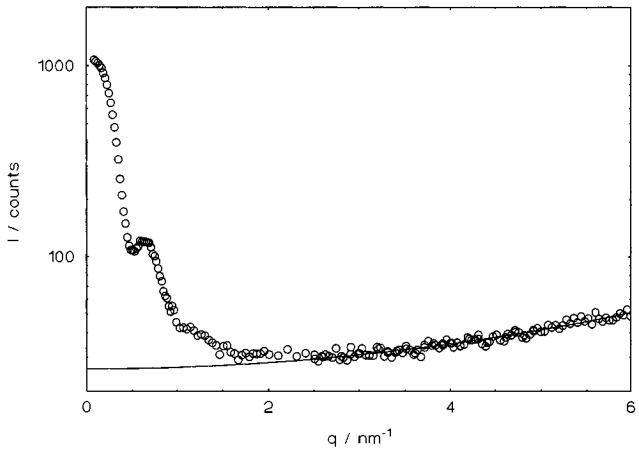

Figure 2. Subtraction of the scattering background due to density fluctuations by application of eq 2. The circles denote the smeared scattering intensity after subtraction of the contribution due to the solvent. The solid line displays the contribution according to eq 2. The parameters A and B have been determined by a fit of eq 2 to the experimental data between $q = 3$ and 5 nm^{-1}.

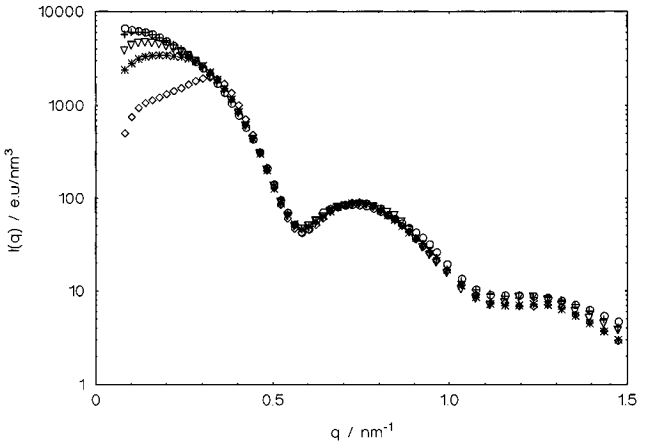

Figure 3. Influence of volume fraction. Desmeared scattering curves measured at different concentration normalized to the volume fraction ϕ. ○, 0.009; ×, 0.017; ▽, 0.043; *, 0.074; ◇, 0.154. In all cases the fluctuation-induced background has been removed (cf. Figure 2). For the sake of clarity only every second point is plotted.

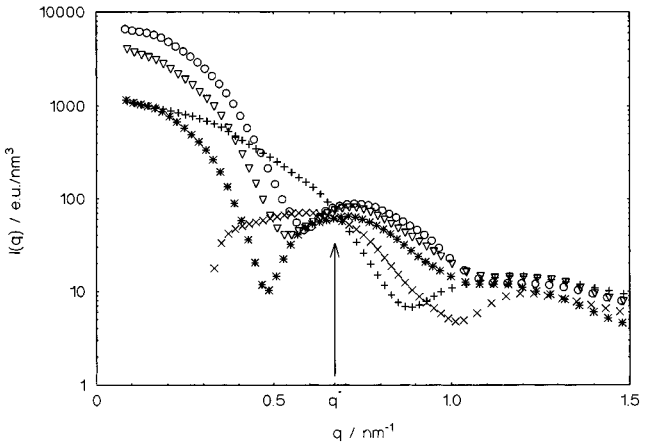

Figure 4. Influence of contrast. Desmeared scattering curves measured at different contrast obtained through addition of glycerol to the solutions. ○, 0% glycerol; ▽, 8.8% glycerol: *, 20.6% glycerol; ×, 33.9% glycerol (near matchpoint); +, 50% glycerol. The arrow marks the $q^* = 0.67$ nm^{-1} of the crossing point (see the text for an explanation).

Figure 2 also displays evidence for a second side maximum of the scattering curves not clearly visible in the corresponding curves in Figure 1b. In this region, however, the contribution of the solvent is considerably higher than that of the micelles and the data are less secure than is the case at lower angles.

The parameter *A*, which is proportional to the fluctuation-induced scattering intensity, scales with the concentration of micelles as expected. From the slope we derive for this contribution 391 eu/nm^3. This value may be compared to the one obtained previously for the fluctuation-induced contribution in polystyrene latexes (430 eu/nm^3, see the discussion of this point in ref 26). The correct dependence on micelle concentration and the reasonable magnitude of the value underscores the validity of the procedure used for removal of this part of the scattering curve.

Results and Discussion

Scattering Curves, General Discussion. Figure 3 displays the resulting absolute scattering intensities obtained for different concentrations of the block copolymer in water divided by the respective volume fraction. In all cases to be discussed from now on the fluctuation background of the micelles has been subtracted. It is evident that all scattering curves coincide except for the region of lowest scattering angles due to the effect of interparticular interference. For small concentrations (<1 vol %), the structure factor is not operative beyond $q = 0.12$ nm^{-1} and may be disregarded in turn.

The variation of the scattering intensities with contrast may be determined by changing the solvent from water to mixtures of water and glycerol. Figure 4 shows the scattering curves measured at five different contrasts (volume fraction of block copolymer 0.9 vol %).

There is a marked variation of the scattering intensities with contrast as expected. The most prominent feature in Figure 4 is the crossing point of all scattering curves at a q^* indicated in the graph. To the authors best knowledge, Philipse, Smits, and Vrij[10] have been the first to point out that such a common point of intersection must exist for well-defined particles provided the polydispersity is not too high. (See also the discussion of this points in refs 20, 27, and 28). Therefore Figure 4 demonstrates that the solutions contain objects with a size distribution being sufficiently narrow.

The data displayed in Figure 4 furthermore suggest clearly that the average electron density does not change upon addition of glycerol. Previous investigations show[1] that the micelles under consideration here consist of a hydrophobic core devoid of solvent and a hydrophilic shell in which the solvent can penetrate. Thus, if the poly(ethylene oxide) chains which extend into the solvent would undergo major changes of conformation upon addition of glycerol, the structure of the particles would be alterated profoundly. Drastic changes would be effected if the glycerol would enter the cores of the micelles, of course. This point discussed qualitatively up to now can be confirmed quantitatively by determination of integral parameters and their variation with contrast.

Evaluation of Integral Parameters. In general, the scattering intensity of a an ensemble of interacting monodisperse particles may be rendered as[14]

$$I(q) = NV_p^2(\bar{\rho} - \rho_m)^2 P(q)S(q) = \phi V_p(\bar{\rho} - \rho_m)^2 P(q)S(q) \tag{3}$$

where N is the number of particles per unit volume, V_p is the volume of the particles, $P(q)$ is the form factor normalized to unity at $q = 0$, and ϕ is the volume fraction of the particles. The quantity $S(q)$ denotes the structure factor of the system, ρ_m is the electron density of the medium, and $\bar{\rho}$ is the average electron density of the particles defined by

$$\bar{\rho} = V_p^{-1} \int_V \rho(r)\, \mathrm{d}V \tag{4}$$

with ρ(r) being the electron density inside the particles.

To assess the influence of the structure factor on the data displayed in Figure 3, it is expedient and permissible to treat the micelles as an ensemble of hard spheres with an effective diameter d of hard-sphere interaction.[21] In this model, d is the minimum distance to which two spheres may approach each other. For the small concentrations under consideration here, binary interactions between the spheres will prevail. For small volume fractions, $S(q)$ may be rendered as (cf. ref 13)

$$\frac{1}{S(q)} = 1 + 2B_{app}\phi \tag{5}$$

with the apparent virial coefficient B_{app} given by

$$B_{app} = 4\frac{(4\pi/3)d^3}{V_p}\cdot\left(1 - \frac{1}{10}d^2q^2 + \ldots\right) \tag{6}$$

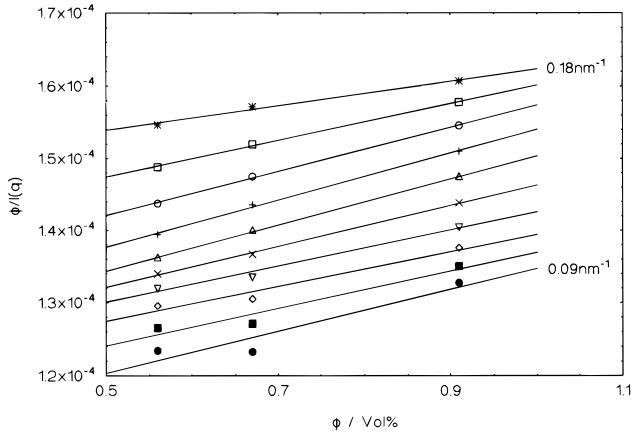

Figure 5. Extrapolation of the scattering intensities at vanishing concentration according to eq 5. The q-values range from 0.09 to 0.18 nm^{-1} in steps of 0.01 nm^{-1}.

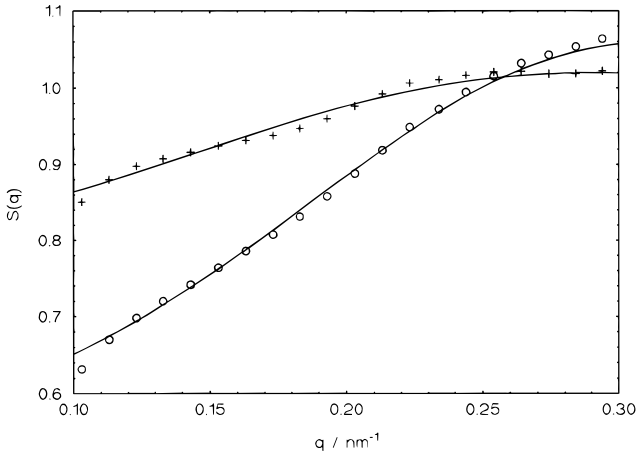

Figure 6. Structure factor of the micelles in the dilute regime at two volume fractions (+, 0.017; ○, 0.043). The solid lines display the fit of the Percus−Yevick structure factor calculated for a system of monodisperse hard spheres.

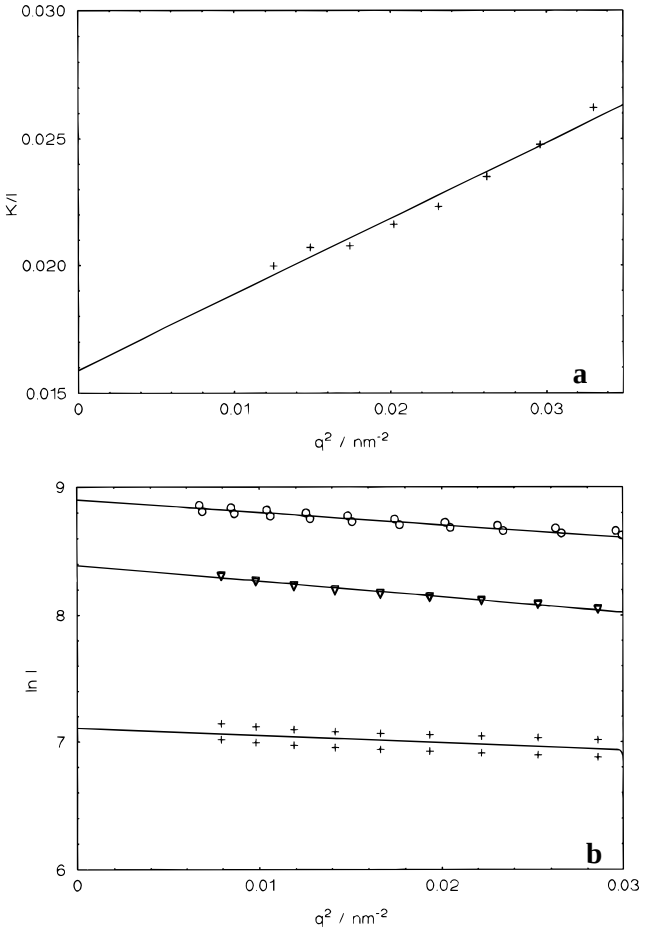

Figure 7. Extrapolation of the scattering intensities according to Zimm (ref 7a) and Guinier (ref 7b). (a) Reciprocal intercepts taken from Figure 5 versus q^2. (b) Guinier plots (eq 8) of data obtained at a volume fraction of approximately 0.9% at three different contrasts. ○, 0% glycerol; ▽, 8.8% glycerol; +, 50% glycerol. The points at a given value of the abscissa refer to repetitions of the measurements.

This suggests the extrapolation of $I(0)$ by plots of $\phi/I(q)$ vs ϕ for given scattering angles. The intercept yields the normalized reciprocal scattering intensity at $q = 0$ whereas the slope of these lines is expected to decrease with q. Figure 5 displays an example for the extrapolation to vanishing concentration.

The values of q accessible by the present SAXS equipment are not small enough to allow the precise determination of d according to eq 6. In order to obtain the effective radius of interaction, the structure factor $S(q)$ is calculated from the experimental data according to eq 3. For a given q the scattering intensities obtained at finite volume fractions are divided through the respective values at vanishing concentration obtained from Figure 5 to yield $S(q)$ displayed in Figure 6. From these data d can be estimated in first approximation by fitting the Percus−Yevick structure factor[29] for a system of monodisperse systems to the experimental data. The solid lines in Figure 6 give the results of such a fit for two concentrations. Agreement is seen over the entire range of q, corroborating the previous result that the system consists of micelles with an effective diameter of interaction.

From these fits $d = 19$ nm, which is higher than the average-diameter of the micelles determined by analysis of the scattering curves (see below). It must be stated in this context, that the present data of $S(q)$ referring to very small concentrations are not accurate enough to allow for an extended discussion. Also, the influence of polydispersity on $S(q)$ has been disregarded. For a more accurate determination of $S(q)$ the region of q must be extended to smaller values to allow the extrapolation of $S(0)$. A more elaborate study of $S(q)$ of these micelles by small-angle neutron scattering is under way.

For noninteracting particles ($S(q) = 1$) and small q, the form factor may be approximated by $P(q) \cong 1 - (1/3)R_g^2q^2$. Therefore the scattering intensity at vanishing scattering angle $I(0)$ can be obtained by

$$\frac{\phi}{I(q,c=0)} \approx \frac{1}{V_p(\bar{\rho} - \rho_m)^2}\left(1 + \frac{R_g^2}{3}q^2\right) \qquad (7)$$

where R_g^2 denotes the radius of gyration. Figure 7a displays the Zimm plot of intercepts of the plot in Figure 5, which correspond to scattering intensities extrapolated to vanishing concentration. Good linearity is observed and the radius of gyration results to 5.8 nm. The contrast factor $\bar{\rho} - \rho_m$ may be calculated[23] from the known chemical composition and the partial specific volume v_2 of the micelles according to $\bar{\rho} - \rho_m = z/v_2 - \rho_m$ (=0.05 e^-/nm^3) with z being the number of electron per gram of block copolymer. From these data V_p is given by 940 nm^3.

This figure, however, results from a small difference of much larger numbers. The value of V_p can be derived from contrast variation (see below), which allows the separate determination of V_p as well as of $\bar{\rho} - \rho_m$. This

Table 1. Integral Parameters of the Micelles Derived from Contrast Variation

ϕ, vol %	glycerol content, wt %	$\bar{\rho} - \rho_m$, nm^{-3}	R_g,[a] nm	$I(0)$,[a] eu/nm^{-3}	$Q/(\phi(1-\phi))$, eu/nm^{-6}	l_c,[b] nm	l_c,[c] nm
0.56	0.0	26.3	5.5	4852	12000	9.0	9.3
0.68	0.0	26.3	5.5	5769	12400	8.4	
0.91	0.0	26.3	5.4	7298	12500	7.8	
1.73	0.0	26.3			13300	7.8	
4.29	0.0	26.3			12700	8.1	
7.43	0.0	26.3			12200	7.7	
15.4	0.0	26.3			11200	6.4	
0.9	8.8	20.2	6.0	4337	9600	7.1	8.4
0.91	20.6	11.4	6.2	1327	5500	4.6	5.9
0.9	33.9	1.5			3000	2.9	3.3
0.92	50.0	−10.6	4.3	1228	4400	6.5	7.1

[a] $I(0)$, R_g determined by the Guinier plots (Figure 7b). [b] Determined experimentally. [c] Calculated from model II.

method seems to be more reliable and the resulting value of V_p is used in turn.

Alternatively, $I(0)$ and the radius of gyration may be obtained by the Guinier extrapolation:[13−15]

$$\frac{I(q)}{\phi} = V_p(\bar{\rho} - \rho_m)^2 \exp\left(-\frac{R_g^2}{3}q^2\right) \quad (8)$$

Figure 7b gives the resulting Guinier plot of data measured at 0.9 vol % for three different contrasts. The respective radii of gyration are gathered in Table 1.

The Zimm extrapolations to vanishing q and volume fraction displayed in Figures 5 and 7a are rather laborious and require measurements at several concentrations. The value deduced from this procedure is slightly higher than the respective values taken from the Guinier extrapolation at finite concentrations. The difference in the radius of gyration obtained by these extrapolation procedures has been discussed repeatly in literature (see, e.g., ref 30). It may be traced back to the influence of the structure factor but also to the effect of the size distribution. It may be disregarded, however, when discussing the strong variation of $I(0)$ and the radius of gyration with contrast. Therefore all data for $I(0)$ and R_g to be discussed further have been obtained by the Guinier extrapolation.

The normalized scattering intensity $I(0)/\phi$ allows determination of the average electron density of the particles since

$$\left[\frac{I(0)}{\phi}\right]^{1/2} = (\bar{\rho} - \rho_m)V_p^{1/2} \quad (9)$$

Figure 8 demonstrates that this relation is fulfilled in excellent accuracy. Here $I(0)$ has been taken from the Guinier extrapolation (cf. Table 1). From this plot the average electron density is given by 359.7 nm^{-3}. The volume of the particles results to 1175 nm^{-3}, which would correspond to a sphere of radius 6.6 nm. The apparent weight-average molecular weight calculated from this figure amounts to 800.000 g/mol, which corresponds to an association number of 400.

The strict linearity of $I(0)$ with the excess electron density as well as the existence of a crossing point of the scattering curves (see above) shows most clearly that the micelles under consideration here present a system of defined and stable particles. This fact leads unambiguously to the conclusion that the change of contrast did not lead to a change of the average electron density of the particles. A similar finding has been reported by Paradies[12] in the course of a fundamental study of micelles of comparable composition formed by a nonionic surfactant in water.

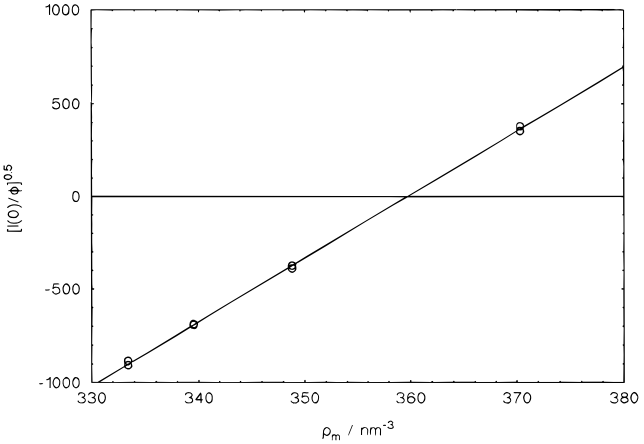

Figure 8. Dependence of $I(0)$ on the electron density ρ_m of the solvent according to eq 9. The points at a given value of the abscissa refer to repetitions of the measurements.

The dependence of the scattering intensity on contrast can be put into more quantitative terms by decomposing it into a form part and a part due to the internal variation of electron density. As discussed recently,[20] the local electron density (cf. also ref 31) of the particles $g(\vec{r}, \rho_m)$ may be split into an external and an internal part by

$$g(\vec{r}, \rho_m) = \rho(\vec{r}) - \rho_m = \phi(\vec{r})[\bar{\rho} - \rho_m] + \phi(\vec{r})\Delta\rho(\vec{r}) \quad (10)$$

Here $\phi(\vec{r})$ denotes the shape function[19,20] of the particles, $\bar{\rho}$ is the average electron density of the particles, and $\phi(r)\Delta\rho(\vec{r})$ is the internal variation of the electron density independent of external contrast. For objects with sharp surfaces, the shape function can only assume the value 1 inside the particle and 0 outside. Following Feigin and Sholer[19] $\phi(\vec{r})$ is allowed to vary continuously between 0 and 1 to account for the finite resolution of the SAXS experiment.[20]

From eq 10 it follows that the intensity $I(q)$ has three contributions:

$$I(q) = (\bar{\rho} - \rho_m)^2 I_S(q) + (\bar{\rho} - \rho_m)I_{SI}(q) + I_I(q) \quad (11)$$

Here $I_S(q)$ refers to the scattering intensity due to the shape of the particles, i.e., of an object with homogeneous excess electron density $\bar{\rho} - \rho_m$, the shape of which is characterized by the shape function $\phi(\vec{r})$. The term $I_I(q)$ refers to the Fourier-transform of internal electron density as defined through eq 10. The third contribution $I_{SI}(q)$ is the respective cross term.

From the discussion in ref 20 it follows that the position q^* of the crossing point is the position the minimum of the form contribution $I_S(q)$. Hence, assuming a monodisperse system of spherical particles with radius R, the form contribution will vanish at q^*R = 4.4934, 7.7253, ..., where q^* is given by the condition $q^*R = \tan(q^*R)$.[10] From the crossing point at $q^* = 0.67$ nm^{-1}, a radius of 6.6 nm can be estimated, which coincides with the value deduced from V_p (see also the discussion of this problem in ref 27). This provides additional evidence that the micelles must have an overall spherical shape.

The dependence of the radius of gyration R_g^2 on contrast provides another stringent test for the applicability of contrast variation to the micelles investigated here. From eq 10 it follows that[31,13,20]

$$R_g^2 = R_{g,\infty}^2 + \frac{\alpha\bar{\rho}}{(\bar{\rho} - \rho_m)} - \beta(\bar{\rho} - \rho_m)^{-2} \qquad (12)$$

Here $R_{g,\infty}^2$ denotes the radius of gyration at infinite contrast, i.e., of the shape function, whereas the coefficient is given by

$$\alpha = (\bar{\rho}V_p)^{-1} \int_0^\infty \phi(\vec{r})\Delta\rho(\vec{r})r^2 \, dV \qquad (13)$$

and present the second moment of the internal electron density distribution. The contribution of the order $(\bar{\rho} - \rho_m)^{-2}$ is related to the dependence of the center of gravity on contrast. It is expected to vanish for centrosymmetric particles.[13,19]

In Figure 9 the radius of gyration is plotted versus the average excess electron density $(\bar{\rho} - \rho_m)$ of the particles. Here $\bar{\rho}$ has been taken from the plot shown in Figure 8. Strict linearity within experimental uncertainty is seen showing that eq 12 is fulfilled indeed. The radius of gyration at infinite contrast $R_{g,\infty}$ results from this plot to 5.35 nm. For a homogeneous sphere $R^2 = (5/3)R_g^2$, which would give $R = 6.9$ nm. It compares favorably with $R = 6.6$ nm deduced from V_p. This gives a further piece of evidence that the overall shape of the micelles must be spherical. The parameter α amounts to 0.34 nm and gives a measure for the spatial inhomogeneities within the micelle. Since α is a positive quantity the electron density must be higher in the shell of the particles and lower in the core.[31]

Another important piece of information accessible through the small-angle experiment is the invariant Q given by

$$Q = \int_0^\infty I(q)q^2 \, dq = 2\pi^2 \int_0^\infty (\rho(r) - \rho_m)^2 \, dV \qquad (14)$$

As is obvious from eq 14, the determination of the invariant requires reliable scattering data up to high scattering angles. The calculation of Q hence might be disturbed by an incorrect background subtraction. To assess this problem in more detail, Q has been determined for a set of data for which different methods of subtracting the fluctuation-induced background have been applied. From this comparison Q may be estimated to be afflicted by an error of the order of 20% at most. In the region of small angles the Guinier extrapolation is used to complement the data. The influence of the structure factor can be disregarded because of the weighting of the data by q^2. Thus, for the micelles under consideration here, the entire relevant range of q is accessible, allowing the determination of the invariant with sufficient accuracy.

Insertion of eq 10 into 14 leads to

$$Q = 2\pi^2 V_c[(\bar{\rho} - \rho_m)^2 + 2(\bar{\rho} - \rho_m)\overline{\Delta\rho} + \overline{\Delta\rho^2}] \qquad (15)$$

where the volume V_c is defined by

$$V_c = \int \phi^2(\vec{r}) \, d\vec{r} \qquad (16)$$

and the coefficients $\overline{\Delta\rho}$ and $\overline{\Delta\rho^2}$ through

$$\overline{\Delta\rho} = \frac{1}{V_c}\int \phi^2(\vec{r})\Delta\rho(\vec{r}) \, d\vec{r} \qquad (17)$$

and

$$\overline{\Delta\rho^2} = \frac{1}{V_c}\int \phi^2(\vec{r})\Delta\rho^2(\vec{r}) \, d\vec{r} \qquad (18)$$

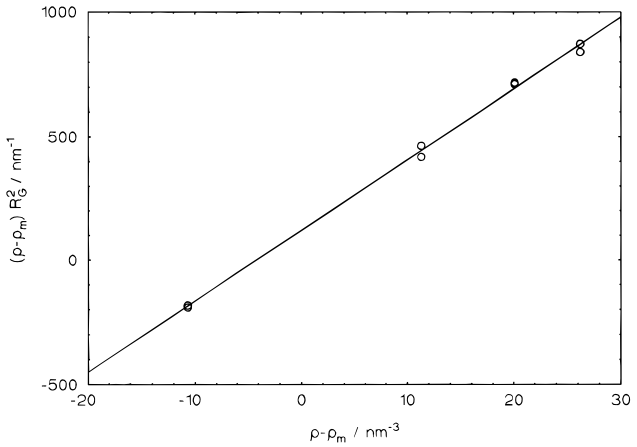

Figure 9. Dependence of the radius of gyration on contrast according to eq 12. The points at a given value of the abscissa refer to repetitions of the measurements.

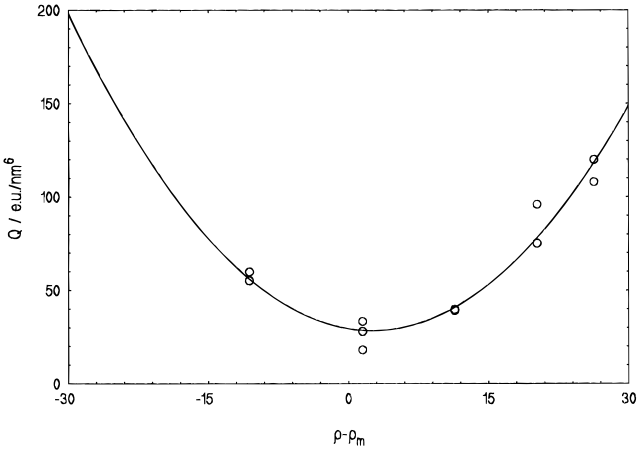

Figure 10. Dependence of the invariant on contrast according to eq 15. The points at a given value of the abscissa refer to repetitions of the measurements. The solid line displays the fit in powers of $\bar{\rho} - \rho_m$ according to eq 15.

The coefficient $\overline{\Delta\rho}$ will vanish[20] for particles characterized by a discontinuous shape function $\phi(\vec{r})$. The volume V_c is in general smaller than V_p since eq 16 presents the volume integral over $\phi^2(\vec{r})$ whereas V_p is given by the volume integral over $\phi(\vec{r})$. Only for particles with sharp boundaries the resulting V_c is equal to V_P.

As lined out in ref 20, precise measurements of the invariant as a function of contrast may serve for an experimental investigation of the coefficients $\overline{\Delta\rho}$ and $\overline{\Delta\rho^2}$. Since $\bar{\rho} - \rho_m$ can be determined with great precision through application of eq 9, Q can be plotted against contrast according to eq 15. A continuous shape function will give a term linear in contrast, which changes its sign when going from positive to negative contrast.

Figure 10 demonstrates that the invariant can be described well by eq 14. The volume V_c is found to be indeed slightly smaller than V_p (cf. Table 2) and the data point to a slight asymmetry with regard to the sign of the contrast; i.e., there is clear evidence for a nonzero coefficient $\overline{\Delta\rho}$ as defined by eq 17 ($\overline{\Delta\rho} = -2.35$ nm^{-3}, see Table 2). As expected from the considerations in ref 20, the shape function of the micelles under consideration here exhibits a continuous character. It will be shown below that the micelles are composed of a solid core and a corona where the ethylene oxide chains protrude into the water phase. The latter parts of the

Table 2. Comparison of Measured and Calculated Integral Parameters Derived from Contrast Variation

	measured	model I	model II
V_p, nm^3	1175	1500	1237
V_c, nm^3	985	1500	1074
$\bar{\rho}$, nm^{-3}	359.7	359.3	359.7
$\overline{\Delta\rho^2}$, nm^{-6}	212	168	197
$R_{g,\infty}$, nm	5.35	5.68	5.44
α, nm^2	0.34	0.35	0.32
$\overline{\Delta\rho}$, nm^{-3}	−2.35	0.0	−2.39

micellar structure present entities of a size below the limits of resolution of the SAXS experiment. Hence, these feature must be described by a continuous shape function in agreement with the above experimental results.

For a strict two-phase system, the invariant Q must scale with $\phi(1-\phi)$ regardless of the distribution of the material in space.[11] Here we deal with an ensemble of objects which exhibit an internal variation of the electron density as well. At high contrast, however, Q divided by $\phi(1-\phi)$ should be independent of concentration since the form part $I_S(q)$ will govern the scattering intensity. Therefore the data in the sixth column of Table 1 have been divided by this factor. It is seen that at the maximum contrast possible in the present system, i.e., for measurements of the micelles in pure water, $Q/\phi(1-\phi)$ does not depend on ϕ, at least for small concentrations. At higher volume fractions the contribution of $\phi(r)\Delta\rho(\vec{r})$ to the invariant will come into play and cannot be disregarded anymore.

A further integral parameter characterizing the particles is the correlation length l_c, which is the weight-average chord length in a particle of homogeneous excess electron density.[15] It is given by the integral over the autocorrelation function of the electron density and is accessible from experimental data through[13]

$$l_c = \frac{\pi}{Q}\int I(q)q \, dq \tag{19}$$

If the excess electron density within the particles is not constant the autocorrelation function can be decomposed into three terms through use of eq 10. As a consequence, l_c consists of three contributions which may assume negative values (cf. the discussion in ref 13). Therefore l_c is an integral parameter whose variation with contrast defies direct interpretation. For homogeneous spheres of radius R with homogeneous electron density, l_c is given[13] by $3/2R$. At high contrast this parameter may be used to estimate the overall dimensions of the object under consideration. Under these conditions the correlation length probes the average spatial extensions of the shape function. In general, l_c may be used to compare theoretical models to experimental results.

In contrast to the calculation of Q (eq 14), where the small-angle region is damped by the factor q^2, the calculation of l_c from experimental data according to eq 19 is more sensitive to concentration. This is directly obvious when looking at the experimental data displayed in Table 1 which show a decrease of l_c with increasing volume fraction. In the region of small concentrations this effect may be assigned to a non-negligible influence of the structure factor. Hence, a quantitative comparison of theory and experiment would require data which are extrapolated to vanishing concentration.

Modeling of the Internal Electron Density Distribution. The previous discussion has shown that the various structural parameters obtained above clearly point to a spherical shape of the micelles. The internal structure can be described by a spherically symmetric electron density distribution $\rho(r) - \rho_m$, which directly leads to the normalized scattering intensity through[13,14]

$$I(q) = \left[4\pi\int_0^\infty [\rho(r) - \rho_m] r^2 \frac{\sin qr}{qr} \, dr\right]^2 = [B_o(q) + \epsilon(q)]^2 \tag{20}$$

Here the amplitudes $B_o(q)$ and $e(q)$ refer to the Fourier transforms of the shape function and the variation of the internal electron density, respectively:[17]

$$B_o(q) = [\bar{\rho} - \rho_m)]4\pi\int_0^\infty \phi(r) r^2 \frac{\sin qr}{qr} \, dr \tag{21}$$

$$\epsilon(q) = 4\pi\int_0^\infty \phi(r)\Delta\rho(r) r^2 \frac{\sin qr}{qr} \, dr \tag{22}$$

As described previously[17,18,28] the experimental data can be modeled by assuming trial functions for the radial shape function $\phi(r)$ and for $\phi(r)\Delta\rho(r)$, insertion into (21) and (22), and comparison with experimental scattering intensities. Polydispersity may be introduced by adding up the intensities of the different sizes weighted by their respective number density.[17] It is quite obvious, however, that in principle different models can well describe the same scattering intensities. The results from such an indirect determination of the radial electron density must therefore be regarded with caution if only one contrast has been used for its derivation. On the other hand, the data discussed herein derive from five different contrasts. In addition to this, the scattering intensities have been obtained from the entire relevant range of scattering vectors q, thus allowing the determination of all possible integral parameters. Therefore the present discussion of the radial electron density is less prone to artifacts and can be done with sufficient precision.

To illustrate this approach, two models will be discussed here: model I is a core−shell model of the electron density whereas model II takes into account the smooth transition between core and shell and between the shell and the water phase.

Model I. First we try to fit a core−shell model with a core of PS and PEO in the shell as was done by other authors (see, e.g., ref 4). The fit leads to the following results: The weight-average diameter of the core is 12.5 nm and the overall diameter 14 nm. The standard deviation of the size distribution amounts to 12.3%. This model describes very well the scattering curves at high contrast. Only at low contrast there are marked deviations from theory and experiment (Figure 11). In particular, the volumes V_p and V_c cannot be reconciled with this model (cf. Table 2).

Model II. In the next step a linear decrease of the shell density to the solvent was assumed. Since it is still not possible to describe all the curves with such a model, a diffuse boundary[18] between core and shell is introduced. Figure 12 illustrates the radial structure of the micelles (upper part) and the corresponding excess electron density in water (lower part, right-hand side) resulting from the fit of model II. The micelles have a core with a weight-average radius of 5.9 nm, which consists 70% of PS and 30% of PEO. For $r > r_a$ (Figure 12, $r_a = 3.35$ nm) the amount of PEO is increasing with increasing radius. The decrease of the electron density in the corona of the PEO-chains is taken proportional to r^{-3}. The mean thickness of the shell is 1.8 nm and the entire number-average diameter is 15.4 nm. The

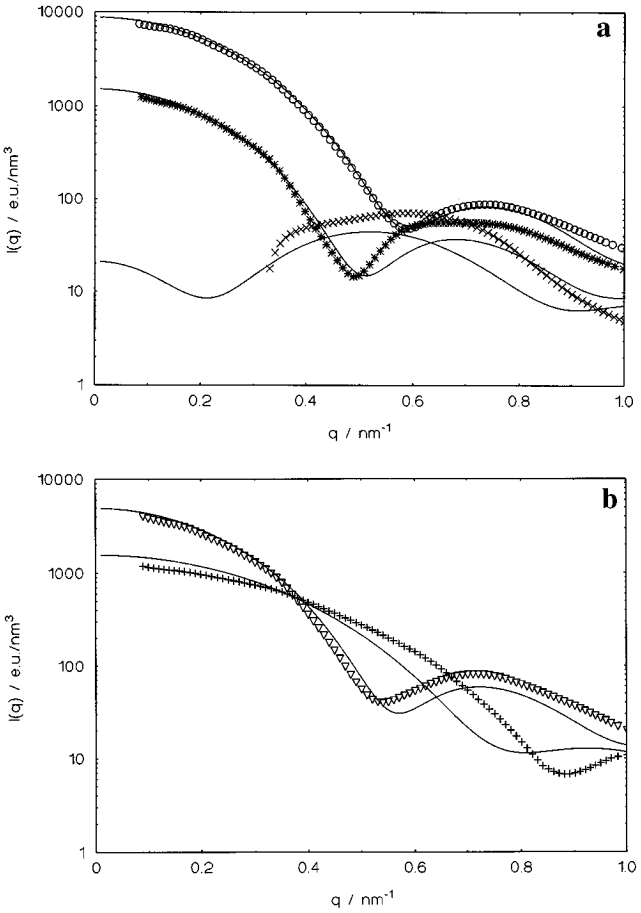

Figure 11. Comparison of the experimental scattering curves with the result calculated for a core−shell model of the radial excess electron density. The numbers in parentheses denote the average excess electron density $\rho - \rho_m/\mathrm{nm}^{-3}$. ○, 0% glycerol (26.3); ▽, 8.8% glycerol (20.2); *, 20.6% glycerol (11.4); ×, 33.9% glycerol (1.5; near matchpoint); +, 50% glycerol (−10.6).

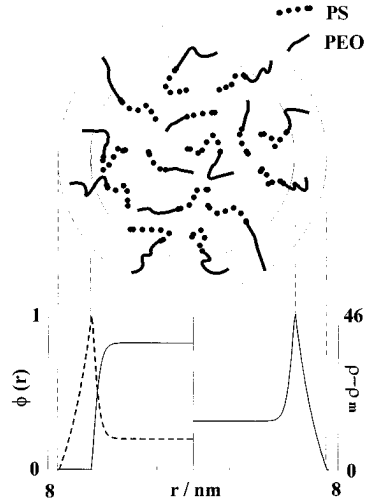

Figure 12. Model of the radial structure of the micelles (upper part) and the corresponding excess electron density in water (lower part, right-hand side). The curve on the left-hand side of the lower part shows the volume fraction of the unpolar component poly(styrene) (solid line) and of poly(ethylene oxide) (dashed line).

amount of solvent in the shell is about 35% of the whole micelle volume. For the size distribution related to the outer diameter of the micelles, a standard deviation of 10.9% is obtained. The polydispersity of the core diameters was found to be less influential and could be neglected in the fit model. The curve in the left-hand side of the lower part shows the volume fraction of the

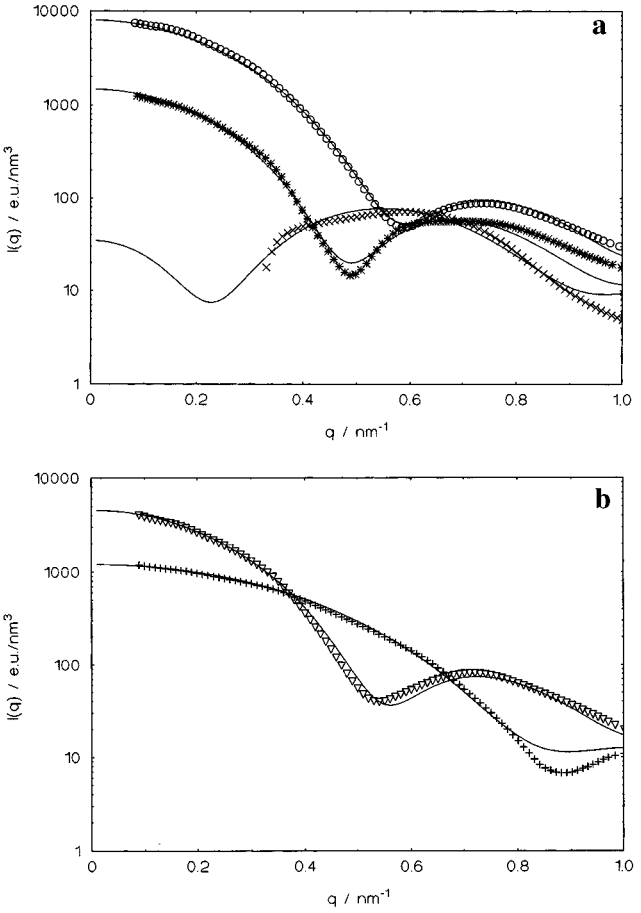

Figure 13. Comparison of the experimental scattering curves with the result calculated for the model of the radial excess electron density displayed in Figure 12. The numbers in parentheses denote the average excess electron density $\rho - \rho_m/\mathrm{nm}^{-3}$. ○, 0% glycerol (26.3); ▽, 8.8% glycerol (20.2); *, 20.6% glycerol (11.4); ×, 33.9% glycerol (1.5; near matchpoint); +, 50% glycerol (−10.6).

unpolar component poly(styrene) (solid line) and of poly(ethylene oxide) (dashed line).

The respective scattering curves calculated according to eq 20 are displayed in Figure 13. This fit is much better than the one by a core−shell model (Figure 11) and there is good agreement of the measured and calculated integral parameters. A comparison of these parameter is given in Tables 1 and 2. There is only some discrepancy regarding the correlation length l_c, which may be due to finite concentrations as already discussed above. Also, the average quadratic electron density $\Delta\rho^2$ deviates in both models from the measured value. It must be kept in mind, however, that this quantity is afflicted by the rather large error incurred in the determination of invariant Q.

It may appear that the number of adjustable parameter necessary in model II is quite high and not fully justified by the experimental data. It must be noted, however, that the parameters used for modeling of the scattering intensities must be compatible with (i) the chemical composition, (ii) the density of the particles, and (iii) the weight concentration of the block copolymers. This imposes severe restrictions to the choice of model parameters.

Model II displayed in Figure 12 leads to the conclusion that there is a surprisingly large fraction (ca. 30%) of the polar material buried in the unpolar core. This can be concluded also from the fact that the poly(styrene) chains of molecular weight 1000 are too short to form a

core of 11.8-nm diameter. Also, the tendency for demixing will be less pronouced than observed for longer chains.

Another argument derives from the density of the contituents: Taking the density of solid polystyrene (1.049 g/cm^3, ref 29), the association number of 400, and the weight fraction of poly(styrene) in the block copolymer, a diameter of 10.6 nm would result for a pure poly(styrene) core. The present data rule out such a small diameter. This conclusion is not related to the validity of the modeling used for fitting the data since the description of the data in terms of model I arrives at approximately the same core size. Thus, it is evident that the core must consist of 28% polar material in good agreement with model II.

The scattering intensity $I_0(q)$ (see eq 11) which governs the scattering intensity at higher angles is mainly due to the strong variation of the electron density at the transition from core to shell and within the shell. It is therefore evident that these features of the internal structure can be determined in a rather accurate fashion. On the other hand, a slow variation of electron density within the core cannot be distinguished from the constant value assumed in model II (cf. Figure 12). It must be kept in mind that model II describes the present results very well, but a more complicated model may be compatible with the scattering intensities as well. As a consequence, a small variation of the electron density within the core cannot be ruled out. This points to the limitations of a small-angle analysis of such objects, which persist despite the fact that the contrast has been varied widely.

It seems that a number-average outer diameter of the micelles of 15.4 nm is difficult to reconcile with the effective diameter d of interaction of 19 nm estimated from the structure factor (see above). The repulsive interaction, however, may be more sensitive toward extended conformations and longer chains may be more important for the effective diameter than for the electron density in the shell. As already mentioned above, d is subject to a rather large experimental error and a quantitative discussion of $S(q)$ must wait for further study of the small-angle region, preferably with small-angle neutron scattering.

Conclusion

First of all, the above discussion has shown that the added glycerol changes only the contrast between the particles and the solvent but not the structure of the particles themselves. Since the scattering data could be determined throughout the entire range of q for all contrasts, including the match point, a number of important integral parameters could be obtained. All data demonstrate unambiguously that we deal with a system of well-defined particles of approximately spherical shape.

Given the spherical symmetry of the micelles, the marked variation of the scattering intensity with contrast also allows the modeling in terms of concentric models of the radial electron density. The internal structure of the particles displayed in Figure 12 shows that the micelles must be regarded as rather disordered systems since a considerable fraction of the polar material is buried in the core. Also, the transition from core to shell as well as the structure of the shell itself points to gradual transitions rather than to steep profiles (cf. the comparison of models I and II). It is evident that in this particular case where all information accessible through a small-angle experiment is available, a full structural analysis of the micelles can be done.

Acknowledgment. We are indebted to N. Dingenouts for helpful discussions. Financial support by the Deutsche Forschungsgemeinschaft, by the Bundesministerium für Bildung und Forschung, by the EG (PROCOPE-project), and by the AIF (Project 9749) is gratefully acknowledged.

References and Notes

(1) Brown, R. A.; Masters, A. J.; Price, C.; Yuan, X. F. In *Comprehensive Polymer Science*; Booth, C., Price, C., Eds.; Pergamon Press: Oxford, U.K., 1989; Vol. 2, Chapter 6.

(2) Tuzar, Z.; Kratochvil, P. In *Surface and Colloid Science*; Matijevic, E., Ed.; Plenum Press: New York, 1993.

(3) Plestil, J.; Baldrian, J. *Makromol. Chem.* **1975**, *176*, 1009.

(4) Chu, B. *Langmuir* **1995,** *11*, 414.

(5) Almgren, M.; Brown, W.; Hvidt, S. *Colloid Polym. Sci.* **1995**, *273*, 2.

(6) Leermakers, F. A. M.; Wijmans, C. M.; Fleer, G. J. *Macromolecules* **1995**, *28*, 3434 and further references given therein.

(7) d'Oliveira, J. M. R.; Martinho, J. M. G.; Xu, Renliang; Winnik, M. A. *Macromolecules* **1995**, *28*, 4750 and further references given therein.

(8) Cogan, K. A., Gast, A. P., Capel, M. *Macromolecules* **1991**, *24*, 6512.

(9) Daoud, M., Cotton, J. P. *J. Phys. (Paris)* **1982**, *43*,531.

(10) Philipse, A. P.; Smits, C.; Vrij, A. *J. Colloid Interface Sci.* **1989**, *129*, 335.

(11) Xu, R; Winnik, M. A.; Riess, G.; Chu, B.; Croucher, M. D. *Macromolecules* **1992**, *25*, 644 and further references cited therein.

(12) Paradies, H. H. *J. Phys. Chem.* **1980**, *84*, 599.

(13) Feigin, L. A.; Svergun, D. I. *Structure Analysis by Small-Angle X-Ray and Neutron Scattering*; Plenum Press: New York, 1987.

(14) Glatter, O.; Kratky, O. *Small Angle X-Ray Scattering*; Academic Press: London, 1982.

(15) Porod, G. In *Small Angle X-Ray Scattering*; Glatter, O.; Kratky, O.; Academic Press, London, 1982, Chapt. 2.

(16) Luzatti, V.; Tardieu, A.; Mateu, L.; Stuhrmann, H. J *J. Mol. Biol.* **1976**, *101*, 115. Luzatti, V.; Tardieu, A. *Annu. Rev. Biophys. Bioeng.* **1980** *9*, 1.

(17) Dingenouts, N.; Ballauff, M. *Acta Polym.* **1993**, *44*, 178.

(18) Dingenouts, N.; Kim, Y. S., Ballauff, M. *Colloid Polym. Sci.* **1994**, *272*, 1380.

(19) Feigin, L. A.; Sholer, I. *Sov. Phys. Crystallogr.* **1975**, *20*, 302.

(20) Hickl, P.; Ballauff, M. *Phys. A*, submitted.

(21) Mortensen, K. *Europhys. Lett.* **1992**, *19*, 599.

(22) Molyneux, P. *Water-Soluble Synthetic Polymers: Properties and Behavior*; CRC Press: Boca Raton, FL, 1983; Vol. 1.

(23) Müller, K.; in Glatter, O.; Kratky, O., *Small Angle X-Ray Scattering*; Academic Press, London, 1982, Chapter 7.

(24) Stabinger, H.; Kratky, O. *Makromol. Chem.* **1978**, *179*, 1655.

(25) Ruland, W. *Colloid Polym. Sci.* **1977**, *255*, 417.

(26) Grunder, R.; Urban, G.; Ballauff, M. *Colloid Polym. Sci.* **1993**, *271*, 563.

(27) Penders, M. H. G. M.; Vrij, A. *Colloid Polym. Sci.* **1990**, *268*, 823.

(28) Bolze, J.; Ballauff, M. *Macromolecules*, in press.

(29) Hansen, J. P.; McDonald, I. R *Theory of Simple Liquids*, 2nd ed.; Academic Press: London, 1986.

(30) Oberthür, R.; Kiste, R. G. in *Small Angle X-Ray Scattering*; Glatter, O., Kratky, O.; Academic Press: London, 1982; Chapter 12.

(31) Stuhrmann, H. B.; Kirste, R. G. *Zeitsch. Phys. N. F.* **1967**, *56*, 334.

(32) Brandrup, J., Immergut, E. H., Eds. *Polymer Handbook*, 3rd ed.; Wiley: New York, 1989.

MA951480V